Heliyon 8 (2022) e11345

Contents lists available at ScienceDirect

Heliyon

journal homepage: www.cell.com/heliyon

Research article

Biophysical insights into the binding capability of Cu(II) schiff base complex with BSA protein and cytotoxicity studies against SiHa

Minakshi Maity [a], Ushasi Pramanik [b], Venkatesha R. Hathwar [c], Paula Brandao [d], Saptarshi Mukherjee [b], Swapan Maity [e], Ribhu Maity [a], Tithi Maity [f], Bidhan Chandra Samanta [a,*]

[a] Department of Chemistry, Mugberia Gangadhar Mahavidyalaya, Bhupatinagar, Purba Medinipur, 721425, West Bengal, India
[b] Department of Chemistry, IISER Bhopal, Bhopal Bypass Road, Bhauri, Bhopal 462 066, Madhya Pradesh, India
[c] School of Physical and Applied Sciences, Goa University, Taleigao Plateau, Goa 403 206, India
[d] Departamento de Química/CICECO, Universidade de Aveiro, 3810-193 Aveiro, Portugal
[e] School of Materials Science and Technology (SMST), Indian Institute of Technology (IIT), BHU, India
[f] Department of Chemistry, Prabhat Kumar College, Purba Medinipur, Contai, 721401, West Bengal, India

HIGHLIGHTS

- Cu(II) Schiff base with four co-ordinations forms distorted square planar geometry.
- The complex can act as promising BSA quencher.
- Cytotoxicity of the complex against SiHa cell by MTT assay.
- Potential as an anti-cancer drug for human cervix uteri carcinoma.

GRAPHICAL ABSTRACT

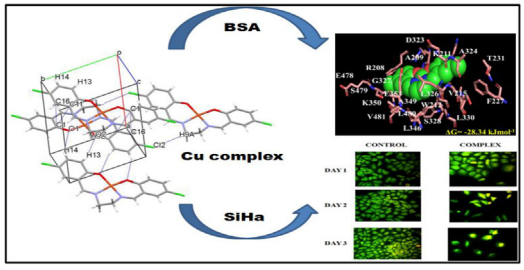

ARTICLE INFO

Keywords:
BSA quencher
Cu(II) complex
Cytotoxicity
Schiff base
SiHa cancer cell

ABSTRACT

Herein, we have explored the effects of chlorinated mononuclear Cu(II) complex upon binding with BSA protein (bovine serum albumin) and its *in vitro* anti-proliferative potentiality against SiHa cell. The complex was synthesized involving a Schiff base ligand having N,N,O donor centers and characterized by several spectroscopic studies. Structure, DFT studies and Hirshfeld surface (HS) analyses were identified using crystallographic computational studies. The binding interaction with BSA depicts the efficacy of the complex towards promising binding of it with BSA. Further, the complex shows a moderate cytotoxicity against SiHa cancer cell signifying its potentiality as an anti-proliferative agent for human cervix uteri carcinoma.

1. Introduction

In recent times, there is a considerable demand for the synthesis of effective anticancer drugs as millions of deaths occurring each year globally are due to cancer [1, 2, 3]. In this regard, the booming discovery of platinum based cisplatin and its analogues as effective anticancer drugs is undoubtedly remarkable. But to avoid the serious remedial drawbacks of platinum based complexes, chemists are prompted to develop non-platinum metal complexes [4, 5]. Thereafter a lot of complexes other than platinum metal are synthesized which are vastly utilized in the field of biology along with anticancer [6], antiseptic [7] and opposed to fungal [8] applications.

* Corresponding author.
E-mail address: bidhansamanta@yahoo.in (B. Chandra Samanta).

https://doi.org/10.1016/j.heliyon.2022.e11345
Received 30 August 2022; Received in revised form 19 September 2022; Accepted 26 October 2022

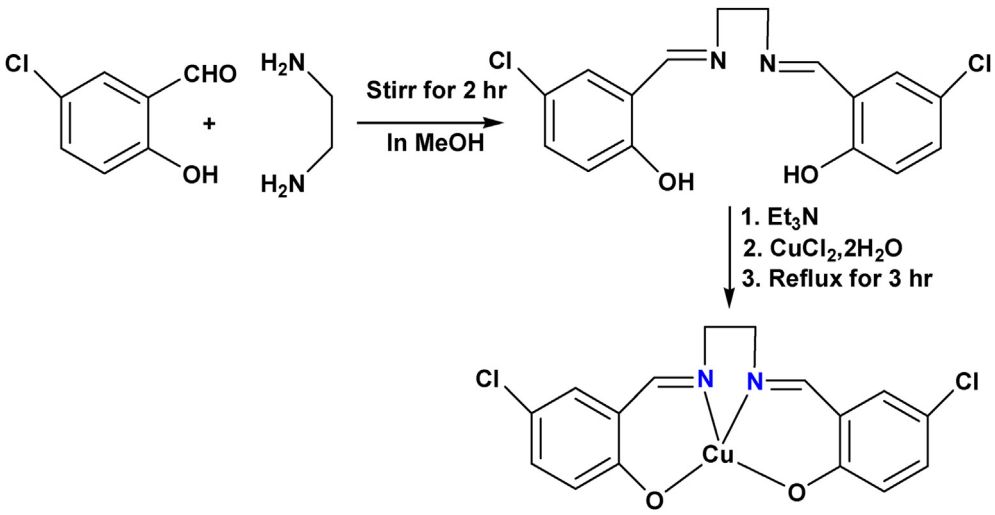

Scheme 1. Schematic representation of ligand and complex preparation.

The major non-platinum complexes that are considered as strong antitumor drugs are copper [9, 10, 11, 12] and ruthenium [13, 14, 15, 16, 17, 18, 19] complexes. Copper, being a vital component, is very much used as catalytic cofactor in various biological pathways [20, 21]. Also, it may be utilized as latent cancer-specific target. A number of copper complexes are now projected as prospective antitumor materials and cancer restraining agents [22, 23, 24, 25, 26, 27, 28], because they reveal outstanding antitumor activity and demonstrate wide-ranging toxicity lower than platinum complexes.

But to explain the effective metabolism and transferring process of any medicine, it is very much important to inspect the binding interaction studies of that medicine with serum albumins. These proteins are studied expansively because of their easy accessibility, high stability, low-priced and extraordinary binding capability with ligand. Besides, albumin plays an important function during the transfer process [29]. So, interaction of drugs with albumin protein might be observed as a replica to get elementary idea about these interactions. Because of structural homology of more than 76% with HSA (Human Serum Albumin), interaction study with BSA was carried out extensively in the past years [30, 31].

The current paper reported the synthesis of a Cu(II) Schiff base complex containing ligand (L) resulting from 5-chloro salicylaldehyde and ethylenediamine. BSA interaction with the complex has been studied by UV-spectrophotometry, fluorescence spectroscopy, circular dichroism spectroscopy and the binding mode is discussed. The focus is also centered in the investigation of cytotoxicity of the said complex on the SiHa cancer cell line.

Table 1. Detailed data related to crystallographic analysis of the complex.

Chemical formula	$C_{16}H_{12}Cl_2CuN_2O_2$
Molecular weight	398.72
Crystal system	Triclinic
Space group	$P-1$
Wavelength (Å)	0.71073
a (Å)	8.2373 (6)
b (Å)	9.4598 (7)
c (Å)	10.9104 (11)
α (°)	64.316 (2)
β (°)	75.922 (4)
γ (°)	79.384 (2)
V (Å^3)	740.14 (11)
Z	2
T (K)	150
μ (mm^{-1})	1.85
Crystal size (mm)	0.22 × 0.12 × 0.03
T_{min}, T_{max}	0.687, 0.947
Measured reflections	28617
Unique reflections	3943
Observed reflections [$I > 2\sigma(I)$]	3808
R_{int}	0.030
θ range	2.40–29.16
R [$F^2 > 2\sigma(F^2)$], wR (F^2), S	0.019, 0.057, 1.029
No. of parameters	208
H-atom treatment	Constrained
$\Delta\rho_{max}$, $\Delta\rho_{min}$ (e Å^{-3})	0.41, −0.35

2. Materials and methods used

Materials employed in various experiments of current studies are used without further purifications as they are all of pure reagent grade. The reagents like 5-chloro salicylaldehyde, ethylenediamine, methanol, $CuCl_2.2H_2O$, and Et_3N etc. were procured from Merck. BSA purchased from Sigma-Aldrich Chemicals (USA) was prepared from phosphate buffer (PB) of 10 mM concentration to maintain pH 7.4. 5 μM of BSA was utilized for lifetime and steady-state studies whereas 2 μM concentration of BSA was used during CD study.

2.1. Preparation of L

It was made from the reaction of 5-chloro salicylaldehyde (1mmol) and ethylenediamine (1mmol) with stirring for 2 h in methanol solvent. Yellow colour solution was developed and was employed straightforward for complex preparation (Scheme 1).

UV−vis spectra [λ_{max}, nm (ε, L mol^{-1} cm^{-1}); MeOH solution]: 334.4 (5074).

2.2. Preparation of complex

$CuCl_2.2H_2O$ (1 mmol) and ligand L were reacted in methanol to prepare the copper complex under the present study under refluxing condition for about 3 h (Scheme 1). A deep green colour solution was observed. Single crystals of green colour were achieved after few days from slow evaporation technique. These single crystals are finally used for X-ray diffraction.

85% yield. Characteristic FTIR peaks in cm^{-1} for $C_{16}H_{12}Cl_2CuN_2O_2$; (br = broad, s = strong, m = medium, vs = very strong): 3012 (m), 2972 (m), 1313 (s), 1682 (vs), 1209 (s). UV−vis spectra [λ_{max}, nm (ε, L mol^{-1} cm^{-1}); MeOH solution]: 370 (3733).

2.3. Spectroscopic techniques

FTIR study was done in a IR spectrometer (Shimadzu). UV-Vis studies were carried out in a double beam spectrophotometer purchased from Systronic. ESI-MS study for complex was done by mass spectrometer (XEVO G2-XS QTOF).

2.4. Single crystal X-ray diffraction studies

Crystal data collection was performed at 150 K by a graphite monochromated X-ray diffractometer (Bruker Kappa) with Mo-Kα radiation of λ = 0.71073 Å. APEX-II (v2.0-2) program (Bruker) was employed for data processing using φ and ω-scan techniques. For data correction towards Lorentz and polarization effects, SADABS program [32] was used. SHELXT 2014/5 was utilized for solving the structure by direct method and subsequent refinement was performed with the help of F^2 by means of SHELXL2018/3 [33]. Refinement of non-hydrogen atoms was done including parameters related to anisotropic displacement. Thermal parameters used for refinement of hydrogen atoms are 1.2 or 1.5 times greater than subsequent mother atoms. Table 1 shows data and parameters related to crystallographic studies of the complex. The CCDC number, 2165565 is gained from CCDC Centre (Cambridge).

2.5. Hirshfeld surface (HS) analyses

In the solid-state, the complex shows various types of important non-covalent interactions to build the lattice. This knowledge of non-covalent interactions of the complex molecule in solid-state helped to understand their interaction capability and types of interactions with other molecules like protein or small organic molecules. To understand the aforesaid weak intermolecular forces in the crystal in a deeper way, the Hirshfeld surfaces analysis is used as a theoretical tool. With this study, all types of atom-atom short contacts locations can be investigated quantitatively. The Crystal Explorer 3.1 software [34] has been used for quantitative analysis of intermolecular interactions in the crystal structure by HS analysis. The HS analysis involves the partition of electron density (ED) of a molecule into atomic fragments such that a molecule within a crystal is given by a weighting function

$$w(r) = \frac{\sum_{i\in molecule}\rho_i(r)}{\sum_{i\in crystal}\rho_i(r)} = \frac{\rho_{promolecule}(r)}{\rho_{procrystal}(r)}$$

where ρ (r) is a spherically averaged Hartree-Fock atomic ED function of i^{th} nucleus. The cutoff of the weight function is 0.5 Å.

Further, different interactions in the crystal structure have been visualized using different functions such as d_e, d_i, d_{norm}, shape index and curvedness mapped on the HS of the molecules. The normalized contact distance (d_{norm}) in the HS analysis is given by

$$d_{norm} = \frac{d_i - r_i^{vdw}}{r_i^{vdw}} + \frac{d_e - r_e^{vdw}}{r_e^{vdw}}$$

d_e denotes HS distance from nearest nucleus situated outside surface, d_i is the HS distance from nearest nucleus situated inside surface and r^{vdw} corresponds to van der Waals radius. The d_{norm} parameter on the HS of the molecule is visualized in a red-white-blue color code. The corresponding intermolecular contacts which are less than their *vdW* radii are indicated by red regions on the HS. Whereas the blue regions show intermolecular contacts of distance longer than their *vdW* radii. White regions signify that the contact distance is identical to the summation of *vdW* radii. Complementary nature of intermolecular interactions during the packing of molecules is identified by shape index. The curvedness is also useful parameter to understand the interactions such as π…π interactions. The flat regions of a surface are highlighted by a low value of curvedness. Similarly, the 2D fingerprint plot associated with the HS give quantitative information on the percentage contribution of individual interactions to the supramolecular assembly.

2.6. DFT computation calculations

With the help of Gaussian 09 DFT study of the complex was done. Hay double-ζ basis set and effective core potential (ECP) are employed to signify the inner electrons of Cu. Besides, elemental atoms (C, H, N, Cl) were illustrated by 6-31G (d,p) basis sets. For all computations, CPCM (conductor-like polarizable continuum model) was employed. The atomic coordinates of crystallographic structures optimize closed-shell geometry.

2.7. BSA interaction studies

2.7.1. Steady-state experiments

The steady-state measurements were performed by UV–vis spectrophotometer (Cary 100) and Fluorolog 3-111 (Horiba JobinYvon). The fluorescence spectral intensities were modified to avoid the inner filter effect coming from significant absorption of complex below 300 nm (along with the absorption maximum at 370 nm) by using Eq. (1) [35]:

$$F = F_{obs} \times antilog^{(A_{ex}+A_{em})/2} \quad (1)$$

2.7.2. Lifetime studies

Time resolved studies were recorded in time-correlated single-photon counting (TCSPC), λ_{ex} = 295 nm (fwhm~ 800 ps). With DAS-6 software obtained data were deconvoluted by using Eq. (2) [35]:

$$I(t) = \sum_i \alpha_i e^{-t/\tau_i} \quad (2)$$

α_i represents the amplitude of the *i*th lifetime τ_i. The average lifetime $\langle\tau\rangle$ was anticipated by Eq. (3):

$$<\tau> = \frac{\sum_i \alpha_i \tau_i}{\sum_i \alpha_i} \quad (3)$$

2.7.3. CD spectroscopic study

The CD spectra were taken in a spectropolarimeter (JASCO J-815) after correcting baseline at 298 K and using a 0.1 cm cuvette of quartz. The spectra were recorded within the wavelength range of 200–260 nm with a scanning rate of 100 nm min¯1, and each spectrum was as an average of three scans. The obtained ellipticity (θ) was expressed in MRE (Molar Residual Elipticity) and shown in Eq. (4) [36]:

$$MRE = \frac{\theta M}{acl} \quad (4)$$

Here, *M* and *a* denote molecular weight of protein and the number of amino acid residues, respectively. *c*is the concentration in g L^{-1}, and *l* is the path length.

2.7.4. Docking studies

AutoDock 4.2 software was utilized for performing the semi-rigid docking studies [37]. The highest binding energy is well thought-out as the most excellent docked conformer of the ligand. The BSA structure was taken from RCSB protein data bank (PDB ID: 3V03). The ligand molecule (Complex) was optimized in Gaussian 09 software and the

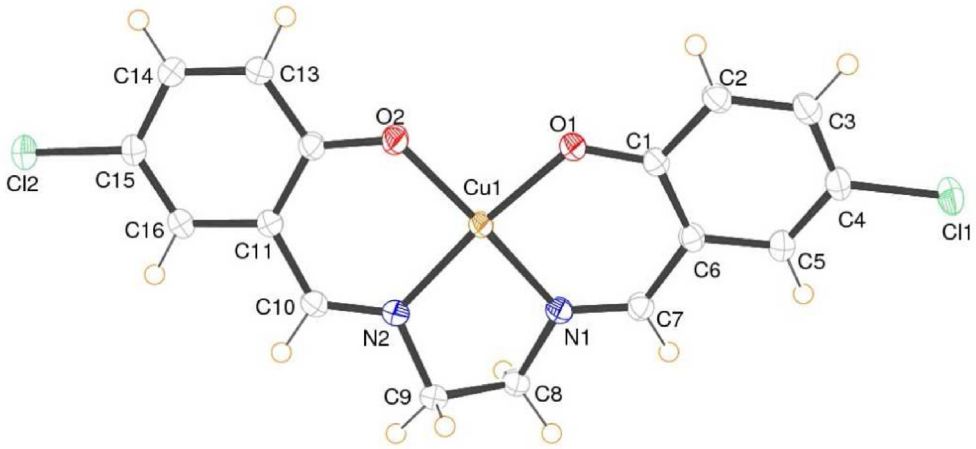

Figure 1. ORTEP plot of the complex with 50% displacement ellipsoids.

optimized structure was further using in docking [38]. The grid sizes along three axes were kept as 126 while the grid spacing was 0.375 Å. The conformation of most excellent docked conformer was examined using PyMOL software [39] out of 50 different conformations.

2.8. Cytotoxicity studies

2.8.1. Culture of cell and maintenance

Dulbecco's Modified Eagle Medium (DMEM) along with 10% heat-inactivated fetal bovine serum (FBS), 100 U/ml penicillin, and 100 μg/ml streptomycin were involved to culture SiHa cells (cancerous tissues of the cervix uteri). 310 K temperature was maintained during culture of the cells in a CO_2 incubator with a 5% CO_2 supply.

2.8.2. Cell proliferation assay

With the help of MTT assay (3-(4,5-dimethylthiazol-2-yl)-2,5-diphenyltetrazolium bromide), the cell proliferation was investigated. Seeding of cell was performed in 0.1 mL of DMEM consisting of 10% FBS, 50 U/mL penicillin and 50 μg/mL streptomycin at the confluences of 70–80% cells per well. These were incubated at 310 K in 5% CO_2. For accuracy in the obtained results all the treatments were performed in triplicate. To remove the dead cells, media of each well were substituted by 100 μL fresh media. Then in order to produce water-insoluble formazan, 0.5 mg/mL of MTT solution in DMEM was supplemented to every well and incubated for extra 3 h at 310 K. This formazan of each well is then mixed with DMSO and absorbance was recorded at 570 nm by a micro plate reader. By using the following formula (Eq. (5)), percentage of cell viability was calculated.

$$\text{Cell viability } (\%) = \frac{OD\ of\ Test}{OD\ of\ Control} \tag{5}$$

where, OD represents specimen optical density.

2.8.3. Fluorescence imaging

A fluorescence microscope was used to visualize cell proliferation efficiency on the specimen. Cancer cells were seeded onto the sample in 12-well plates for 24 h at 310 K. Fresh solution of PBS (phosphate-buffer saline) was used twice to wash test samples for removing the dead or floating cells. The 4% paraformaldehyde solution fixed the adhered cells for 20 min. Then they were washed again with PBS and marked by AO (acridine orange) and EtBr (ethidium bromide) (100 μg/mL) fluorescent dye for 10 min. Again, these were rinsed with PBS for twice and consequently incubated for 5 min in dark. After that with a fluorescence microscope (Leica, Germany) images were collected.

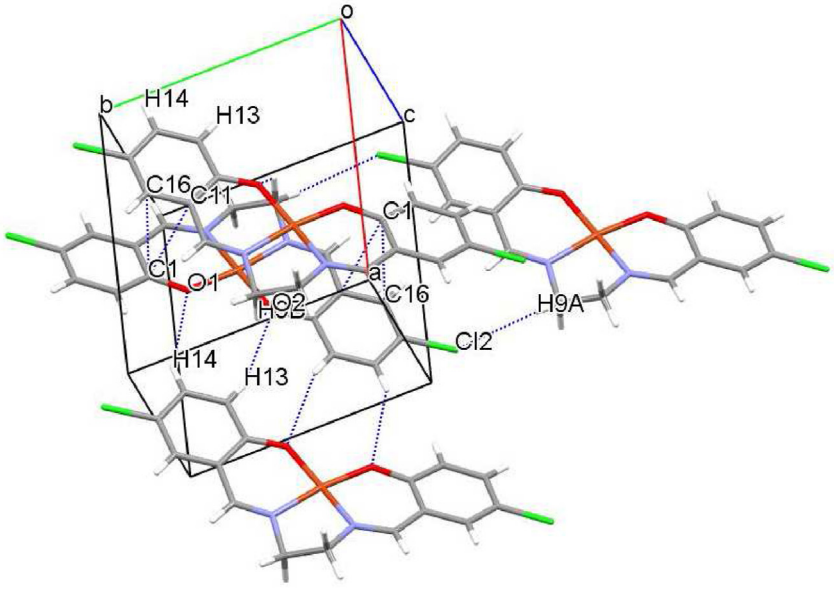

Figure 2. Weak interactions shown in unit cell of complex.

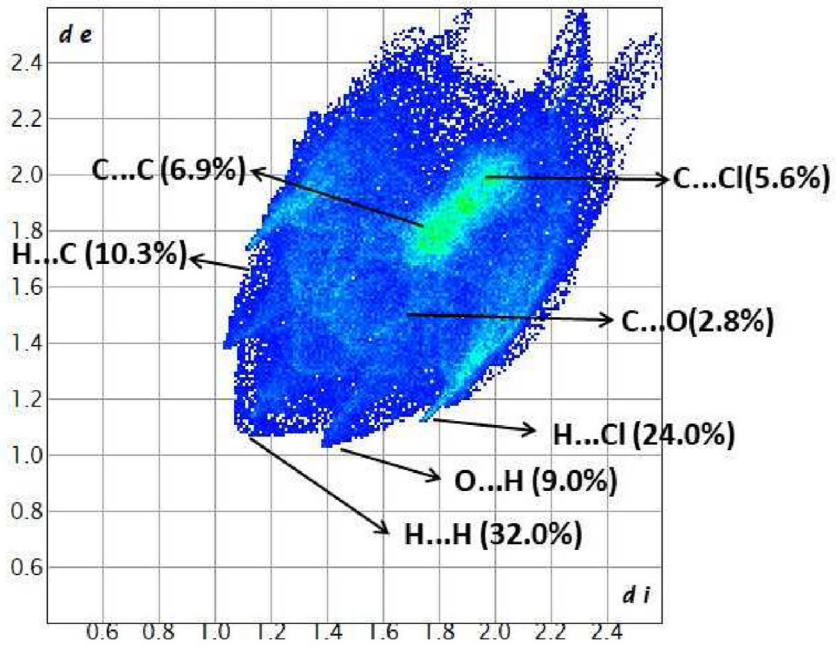

Figure 3. Fingerprint plot obtained from HS analysis.

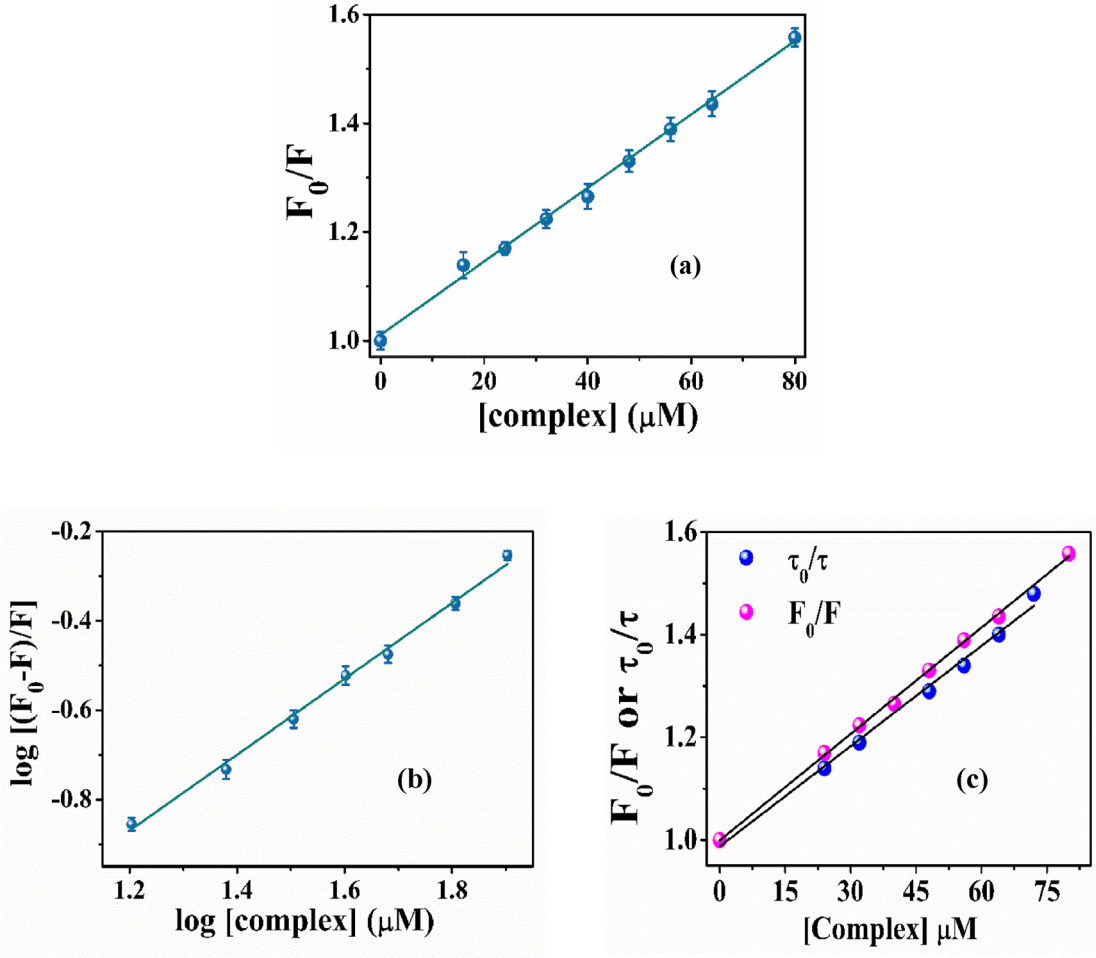

Figure 4. (a) Stern-Volmer plot and (b) modified Stern-Volmer plot of BSA-complex interaction (c) the plot of F_0/F or τ_0/τ as a function of the concentration of complex.

Table 2. Binding parameters of the interaction between BSA and complex.

K_{SV} (M^{-1})	K_b (M^{-1})	n
$(1.01 \pm 0.03) \times 10^6$	$(8.32 \pm 0.45) \times 10^4$	0.94 ± 0.02

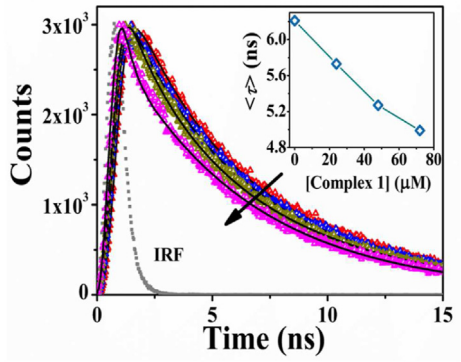

Figure 5. Decay profiles of lifetime in fluorescence at 298 K for 5 μM BSA in nonappearance (red) and appearance of 24 (blue), 48 (dark yellow), 60 (magenta) μM of complex. Instrument Response Function is denoted by IRF. Inset picture shows decrease in average lifetime of BSA with increase in complex concentration.

Table 3. Parameters related to lifetime of tryptophan during interaction between BSA and complex.

System	α_1	τ_1 (ns)	α_2	τ_2 (ns)	$<\tau>$ (ns)
0 μM	0.13	3.10 ± 0.10	0.87	6.67 ± 0.12	6.21 ± 0.08
24 μM	0.15	2.70 ± 0.11	0.85	6.27 ± 0.09	5.73 ± 0.06
48 μM	0.20	2.15 ± 0.09	0.80	6.05 ± 0.10	5.27 ± 0.06
72 μM	0.24	1.90 ± 0.07	0.76	5.96 ± 0.10	4.99 ± 0.05

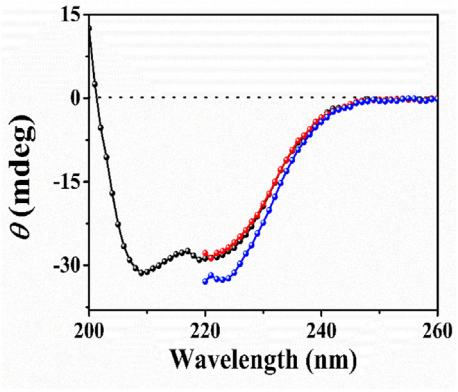

Figure 6. CD spectra represent the helical nature of BSA in the absence of complex (Black) and in the presence of 16 μM (red) and 32 μM (blue) of complex.

3. Analyses of results and discussions

3.1. Structure analyses and spectroscopic characterization

Several techniques of spectroscopy were employed to characterize the synthesized ligand and the complex. The complex structure was firmed and analyzed by X-ray diffraction and HS analyses studies.

The FTIR spectrum is shown in S1 for the complex from which it is observed that the strong peak for azomethine (C═N) group obtained at 1682 cm^{-1} indicating the formation of Schiff base. The other prominent peaks such as C–C at 1209 cm^{-1}, C–H aromatic at 3012 cm^{-1}, C═C at 1313 cm^{-1}, C–H aliphatic at 2972 cm^{-1} and bending peak for C–H at 1343 cm^{-1} which were obtained at their normal areas also support the formation of the complex.

UV–vis results reveal band for π–π* transitions at around 370 nm for C═C and C═N groups in the complex. The band characteristic for ligand appears at 334 nm (n–π*) which is absent in spectrum of complex.

ESI-MS spectra (S2 and S3) for ligand and the complex clearly demonstrate the prominent peaks for expected *m/z* values (slightly different from calculated values) for both ligand and the complex. This slight difference is due to H+ adducts from solvent as the structures of both ligand and the complex contain some probable centre to accept those H+ adducts.

The refinement details related to crystallographic studies are listed in Table 1. The parameters related to geometry of complex show close proximity to the literature values. The crystalline pattern of complex is centrosymmetric with *P*-1 triclinic space group. Crystalline structure contains a central Cu(II) with four co-ordinations resulting in a square planar geometry with distortion (Figure 1 ORTEP diagram). The Cu–N bond lengths at 2.950 (1) Å are somewhat greater with respect to Cu–O bond distances at 1.918 (1) Å. The bond angles such as O–Cu–N, N–Cu–N and O–Cu–O scatter in a wide range between 83.65(4)° and 92.56(4)° indicating that the $\{CuN_2O_2\}$ moiety is distorted (** S1). Both oxygen atoms O1 and O2 participate in the H-bonding with the H atoms of an adjacent molecule (Figure 2 and S2). Additionally, C9–H9A···Cl2 interaction is stabilizing the crystal structure. Strong and weak interactions contributed in lattice are highlighted by HS. Figure 3 represents the contribution of different interactions attained from HS fingerprint plot. The C–H···O and C–H···Cl interactions constitute 33% of total interactions present in the crystal structure. Further, S4 represents Hirshfeld surface obtained by recording d_{norm} (S4a) shape-index (S4b) and curvedness properties (S4c).

3.2. DFT analyses of the complex

The DFT calculations of the complex were performed to understand the electronic construction of the complex. Besides, to get an insight of kinetic stability, chemical reactivity and electrical transport properties of the complex, the understanding of frontier molecular orbitals (HOMOs and LUMOs) is very essential. The small energy gap of HOMO and LUMO orbital of a complex makes it more polarizable. Such molecules are soft molecules that are more capable of chemical and biological reactivity because they have high electron donation (high E_{HOMO}) and acceptor (low E_{LUMO}) ability. MO (molecular orbital) pictures are depicted in S5. As observed from the figure, in HOMO, density of electron is delocalized on the C-centre and the O centers of the salicylaldehyde ring. The same electronic structure was observed in case of single occupied molecular orbital (SOMO). Further, in LUMO the density of electron is localized on C-centers of the salicylaldehyde ring and N centers of the ligand. However, in HOMO -1, the density of electron is transferred to metal centre (i.e., Cu centre) of the complex along with the coordinating atoms of the ligand (N and O). This observation suggests that aromatic rings of the ligand and the metal ions are dynamic parts for biological activities like protein interactions, anti-cancerous properties etc. The HOMO (−6.041 eV) and LUMO (−1.941 eV) molecular orbitals have an energy gap of 4.1 eV indicating capability of the studied complex towards chemical and biological reactivity. The SOMO orbital of the complex is in the energy level of -5.757 eV.

3.3. BSA interaction analyses

BSA shows strong absorption at ~280 nm which increases with increasing concentrations of complex and the complex itself shows absorption around 370 nm (S6a). Upon excitation at 295 nm (which deals exclusively with Tryptophan (W) residue of the protein), the fluorescence

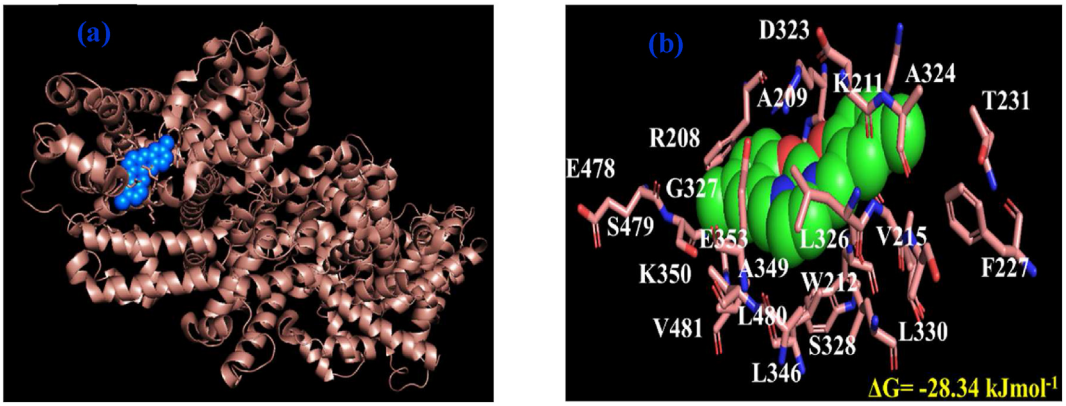

Figure 7. (a) The best docked binding of complex (shown as blue spheres) within BSA (orange ribbons). (b) The amino acid residues of BSA within 8 Å distance from complex.

emission centered at 350 nm decreases (S6b) with addition of complex as a result of Tryptophan quenching [35]. Quenching can be attributed by the formation of complex between the quencher and fluorophore in ground state or due to excited state collision, which can be predicted by the Stern-Volmer Eq. (6) [35]:

$$\frac{F_0}{F} = 1 + K_{SV}[Q] \tag{6}$$

F and F_0 represent intensities of the fluorophore (Tryptophan here) in presence and absence of quencher Q (here the complex) respectively. The plot (Figure 4a) of F_0/F vs. quencher concentration will give a linear nature of the plot from where one can calculate the Stern-Volmer quenching constant (Table 2) [35]. The linearity of the plot gives only one type of quenching phenomenon. The binding parameters were obtained from Eq. (7) below (Figure 4b) and the parameters were tabulated in Table 2:

$$\text{Log}\frac{F_0 - F}{F} = \log K_b + n \log Q \tag{7}$$

K_b denotes binding constant and binding sites number is denoted by n.

To elucidate the exact nature of binding and quenching phenomenon, we further performed time-resolved studies. The lifetime for Tryptophan of BSA in excited state decreases with adding the complex. Reduction in the lifetime values may be attributed by the occurrence of interaction between BSA and complex at excited state by collision and thereby shows reduction in the lifetime of BSA (Figure 5, Table 3). Moreover, we have plotted F_0/F or τ_0/τ as function of complex concentration (Figure 4c), which shows similar trend enabling that the quenching occurs through excited state collision or diffusion. Thus, it can be inferred that the quenching governing the said interaction is dynamic in nature [35].

Furthermore, we have investigated the conformation of the protein upon the said interaction by circular dichroism (CD) spectroscopy. BSA

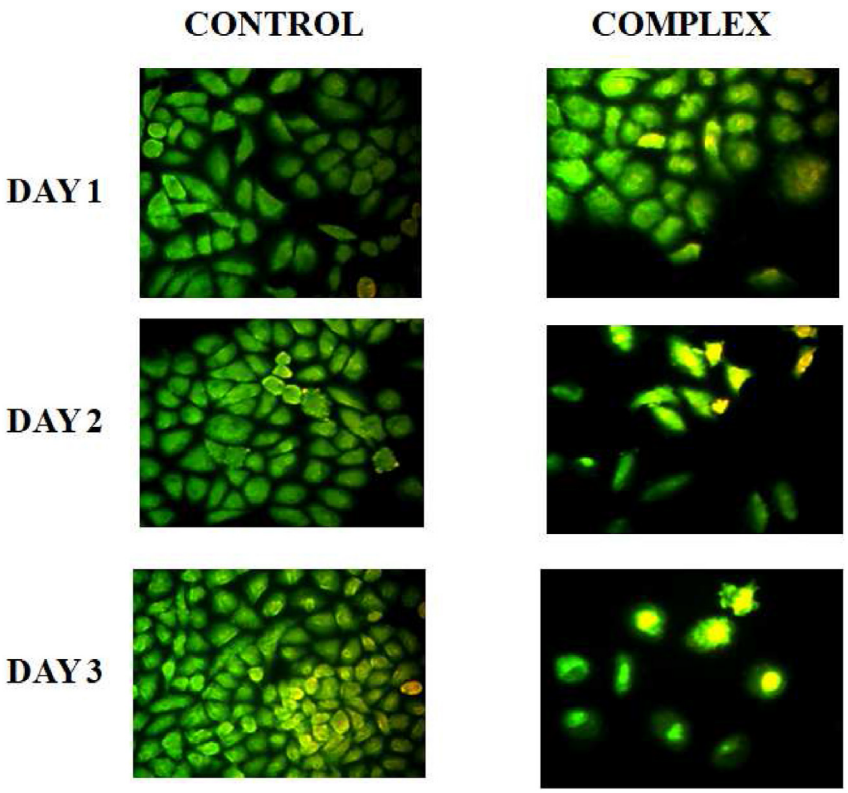

Figure 8. AO/EtBr staining fluorescent images.

shows helical nature in the CD spectra (Figure 6) with two negative ellipticity bands at 222 nm and 208 nm corresponding to n → π* and π → π* transitions, respectively [40]. It is important to note that CD spectra of the protein in presence of complex below 220 nm could not be monitored, as the complex shows strong absorption below this wavelength range and also due to observing high voltage values for the instrumental limitation within the mentioned wavelength range [40].

Besides, to predict the probable binding site of the complex, within the BSA scaffold, we have performed blind docking study. The complex locates itself within BSA where it finds Tryptophan and some hydrophobic amino acid residues of the protein (Figures 7a, b) with binding energy as -28.34 kJ mol^{-1}.

3.4. Cytotoxicity studies

To evaluate cytotoxic effect for studied complex against SiHa, prohibition of cell propagation was checked by nurturing the cells with fixed concentration of the complex for 1, 2, 3 days using MTT assay. As control, the refined cells without sample are taken. About 50 μg/mL of the complex was utilized for this study. S7 shows the results with mean ± 1–1.5 standard deviation values with respect to individual experiments. Gradual decreasing of cell viabilities with time is observed than the control demonstrating cytotoxicity of the complex. To support these data additionally, fluorescent images were collected using AO and EtBr dye. AO and EtBr recognize the normal cells from apoptotic cells on the basis of cell membrane permeability. It is generally observed that AO shows green fluorescence and EtBr demonstrates red fluorescence on binding with DNA. Generally, dead cells shine red and permeable to both the AO and EtBr dye. Whereas, the living cells shine green and permeate only AO. After treatment, the comparative number density of cells can be visualized from fluorescent images of specimen staining with AO/EtBr (Figure 8). It is significant to point out here that the number densities as well as cell health are gradually decreasing owing to the incorporation of the complex into the cells with respect to control and another interesting observation is that cell apoptosis is noticed from day 1 to day 3 gradually indicating green to yellow colour of the cell. So, the complex is significantly cytotoxic in nature showing potential anticancer activity and the cell viability obtained for the complex after days 3 against the cancer cells is very much analogous to the reported values in literature [41, 42].

4. Conclusions

In the current study, synthesis, spectroscopic characterization, structural analyses, Hirshfeld surface, DFT analysis, BSA interaction and cytotoxicity studies of a Cu(II) complex have been investigated. The crystallographic analysis shows that a central Cu(II) with four coordinations results in square planar geometry with distortion. Fingerprint plots of HS analysis exhibit the percentage of various interactions contributed in crystal structure. The C–H···O and C–H···Cl interactions constitute 33% of entire interactions present in the complex. Besides, from DFT study it is revealed that electron clouds of HOMO and LUMO orbitals are dispersed on Cu(II) ions and aromatic rings indicating potential capability of the complex for biological activities like protein interactions, anti-cancerous properties. This inspection leads to examine BSA interaction studies of the complex through a range of spectroscopic studies and the obtained results strongly support the above prediction. Besides, the complex has been found to be significantly toxic for SiHa cancerous cell lines and effectively causes more cell death. Therefore, the complex under the present investigation is expected to show effectual anticancer properties and unlocks the possibility of its uses in chemotherapeutics. The present studies can be expanded to virus infected cell lines which may unfasten a new path in metallopharmaceutics for healing cancer by disturbing life cycle of virus.

Declarations

Author contribution statement

Bidhan Chandra Samanta: Conceived and designed the experiments; Contributed reagents, materials, analysis tools or data; Wrote the paper.

Minakshi Maity, Ushasi Pramanik and Swapan Maity: Performed the experiments.

Venkatesha R. Hathwar, Ribhu Maity and Tithi Maity: Analyzed and interpreted the data.

Paula Brandao: Contributed reagents, materials, analysis tools or data.

Saptarshi Mukherjee: Analyzed and interpreted the data; Contributed reagents, materials, analysis tools or data; Wrote the paper.

Funding statement

Dr. Bidhan Chandra Samanta was supported by Department of Biotechnology, Ministry of Science and Technology, India [HRD-11011/161/2020-HRD-DBT].

Data availability statement

Data will be made available on request.

Declaration of interest's statement

The authors declare no conflict of interest.

Additional information

Supplementary content related to this article has been published online at https://doi.org/10.1016/j.heliyon.2022.e11345.

Acknowledgements

The significant contribution of Dr Debaprasad Mandal (Chemistry, IIT Ropar) regarding FTIR, Mass spectroscopic and DFT studies is highly solicited. Authors wish to thanks to Prof. Pralay Maiti, School of Materials Science and Technology, IIT, BHU for his endless support towards biological studies. Minakshi Maity and Ribhu Maity are thankful to Mugberia Gangadhar Mahavidyalaya for getting facilities related to research works. Ushasi Pramanik wishes to thank IISER Bhopal for generating fellowship.

References

[1] A.K. Rustgi, The genetics of hereditary colon cancer, Genes Dev. 21 (2007) 2525–2538.

[2] F. Islami, A. Goding Sauer, K.D. Miller, R.L. Siegel, S.A. Fedewa, E.J. Jacobs, M.L. McCullough, A.V. Patel, J. Ma, I. Soerjomataram, W.D. Flanders, O.W. Brawley, S.M. Gapstur, A. Jemal, Proportion and number of cancer cases and deaths attributable to potentially modifiable risk factors in the United States, CA, Cancer J. Clin. 68 (2017) 31–54.

[3] G. Jaouen, A. Vessières, S. Top, Ferrocifen type anti cancer drugs, Chem. Soc. Rev. 44 (2015) 8802–8817.

[4] R.F. Brissos, A. Caubet, P. Gamez, Possible DNA-interacting pathways for metal-based compounds exemplified with copper coordination compounds, Eur. J. Inorg. Chem. 16 (2015) 2633–2645.

[5] W.L. Kwong, R.W.Y. Sun, C.N. Lok, F.M. Siu, S.Y. Wong, K.H. Low, C.M. Che, An ytterbium (III) porphyrin induces endoplasmic reticulum stress and apoptosis in cancer cells: cytotoxicity and transcriptomics studies, Chem. Sci. 4 (2013) 747–754.

[6] B. Bertrand, A. Casini, A golden future in medicinal inorganic chemistry: the promise of anticancer gold organometallic compounds, Dalton Trans. 43 (2014) 4209–4219.

[7] T. Stringer, R. Seldon, N. Liu, D.F. Warner, C. Tam, L.W. Cheng, K.M. Land, P.J. Smith, K. Chibale, G.S. Smith, Antimicrobial activity of organometallic isonicotinyl and pyrazinyl ferrocenyl-derived complexes, Dalton Trans. 46 (2017) 9875–9885.

[8] H. Parveen, R.A.S. Alatawi, M.A. Alsharif, M.I. Alahmdi, S. Mukhtar, S.A. Khan, S. Hasan, A.U. Khan, Novel pyrazoline-based organometallic compounds containing

ferrocenyl and quinoline units: synthesis, characterization and microbial susceptibilities, Appl. Organomet. Chem. 32 (2018) 1–8.
[9] P.U. Maheswari, S. Roy, H.D. Dulk, S. Barends, G.V. Wezel, B. Kozlevcar, P. Gamez, J.J. Reedijk, The square-planar cytotoxic [CuII(pyrimol)Cl] complex acts as an efficient DNA cleaver without reductant, J. Am. Chem. Soc. 128 (2006) 710–711.
[10] J.D. Ranford, P.J. Sadler, D.A. Tocher, Cytotoxicity and antiviral activity of transition-metal salicylato complexes and crystal structure of Bis(diisopropylsalicylato)(1,10-phenanthroline)copper(II), J. Chem. Soc., Dalton Trans. 22 (1993) 3393–3399.
[11] C.H. Ng, K.C. Kong, S.T. Von, P. Balraj, P. Jensen, E. Thirthagiri, H. Hamada, M. Chikira, Synthesis, characterization, DNA-binding study and anticancer properties of ternary metal(ii) complexes of edda and an intercalating ligand, Dalton Trans. 2008 (2008) 447–454.
[12] A. Barve, A. Kumbhar, M. Bhat, B. Joshi, R. Butcher, U. Sonawane, R. Joshi, Mixed-ligand copper (II) maltolate complexes: synthesis, characterization, DNA binding and cleavage, and cytotoxicity, Inorg. Chem. 48 (2009) 9120–9132.
[13] A.C.G. Hotze, S.E. Caspers, D. de Vos, H. Kooijman, A.L. Spek, A. Flamigni, M. Bacac, G. Sava, J.G. Haasnoot, J.J. Reedijk, Structure-dependent in vitro cytotoxicity of the isomeric complexes [Ru(L)2Cl2] (L= O-tolylazopyridine and 4-Methyl-2-phenylazopyridine) in comparison to [Ru(azpy)2Cl2], J. Biol. Inorg. Chem. 9 (2004) 354–364.
[14] C.G. Hartinger, S. Zorbas-Seifried, M.A. Jakupec, B. Kynast, H. Zorbas, B.K. Keppler, From bench to bedside–preclinical and early clinical development of the anticancer agent indazolium trans-[tetrachlorobis(1H-indazole)ruthenate(III)] (KP1019 or FFC14A), J. Inorg. Biochem. 100 (2006) 891–904.
[15] M.A. Fuertes, C. Alonso, J.M. Perez, Biochemical modulation of Cisplatin mechanisms of action: enhancement of antitumor activity and circumvention of drug resistance, Chem. Rev. 103 (2003) 645–662.
[16] M. Cocchietto, G. Sava, Blood concentration and toxicity of the antimetastasis agent NAMI-A following repeated intravenous treatment in mice, Pharmacol. Toxicol. 87 (2000) 193–197.
[17] G. Sava, K. Clerici, I. Capozzi, M. Cocchietto, R. Gagliardi, E. Alessio, G. Mestroni, A. Perbellini, Reduction of lung metastasis by ImH[trans-RuCl4(DMSO)Im]: mechanism of the selective action investigated on mouse tumors, Anti Cancer Drugs 10 (1999) 129–138.
[18] B.K. Keppler, M. Henn, U.M. Juhl, M.R. Berger, R. Niebl, F.E. Wagner, New ruthenium complexes for the treatment of cancer, in: E. Baulieu, D.T. Forman, M. Ingelman-Sundberg, L. Jaenicke, J.A. Kellen, Y. Nagai, G.F. Springer, L. Träger, L. Will-Shahab, J.L. Wittliff (Eds.), Prog. Clin. Biochem. Med. 10, Springer, 1989, pp. 41–69.
[19] R.E. Morris, R.E. Aird, P.D. Murdoch, H.M. Chen, J. Cummings, N.D. Hughes, S. Parsons, A. Parkin, G. Boyd, D.I. Jodrell, P.J. Sadler, Inhibition of cancer cell growth by ruthenium(II) arene complexes, Med. Chem. 44 (2001) 3616–3621.
[20] H.B. Kraatz, N. Metzler-Nolte, Concepts and Models in Bioinorganic Chemistry, Wiley VCH, Weinheim, Germany, 2006.
[21] J.J.R. Frausto da Silva, R.J.P. Williams, The Biological Chemistry of the Elements, Clarendon, Oxford, U. K., 1991.
[22] K. Jeyalakshmi, N. Selvakumaran, N.S.P. Bhuvanesh, A. Sreekanth, R. Karvembu, DNA/protein binding and cytotoxicity studies of copper(II) complexes containing N,N′,N′′-trisubstituted guanidine ligands, RSC Adv. 4 (2014) 17179–17195.
[23] B.C. Bales, T. Kodama, Y.N. Weledji, M. Pitie, B. Meunier, M.M. Greenberg, Mechanistic studies on DNA damage by minor groove binding copper-phenanthroline conjugates, Nucleic Acids Res. 33 (2005) 5371–5379.
[24] L. Turecky, P. Kalina, E. Uhlikova, S. Namerova, J. Krizko, Serum ceruloplasmin and copper levels in patients with primary brain tumors, Klin. Wochenschr. 62 (1984) 187–189.
[25] D. Yoshida, Y. Ikeda, S. Nakazawa, Quantitative analysis of copper, zinc and copper/zinc ratio in selected human brain tumors, J. Neuro Oncol. 16 (1993) 109–115.
[26] D.H. Petering, Carcinostatic copper complexes, in: H. Siget (Ed.), Met. Ions Biol. Syst. 11, Marcel Dekker, New York, 1980, pp. 197–229.
[27] O.A. Chaves, I.S. de Castro, C.M. Goulart, M.S. S Bellieny, J.C. Netto-Ferreira, J. Echevarria-Lima, A. Echevarria, In vitro and in vivo cytotoxic activity and human serum albumin interaction for a methoxy-styryl-thiosemicarbazone, Invest. N. Drugs 37 (2019) 994–1005.
[28] T. Miura, A. Hori-i, H. Mototani, H. Takeuchi, Raman spectroscopic study on the copper(II) binding mode of prion octapeptide and its pH dependence, Biochemistry 38 (1999) 11560–11569.
[29] T. Kosta, T. Maryama, M. Otagiri, Species differences of serum albumins: I. Drug binding sites, Pharm. Res. (N. Y.) 14 (1997) 1607–1612.
[30] N. Zhou, Y.Z. Liang, P. Wang, 18b-Glycyrrhetinic acid interaction with bovine serum albumin, J. Photochem. Photobiol., A 185 (2007) 271–276.
[31] L. Shang, X. Jiang, S. Dong, In vitro study on the binding of neutral red to bovine serum albumin by molecular spectroscopy, J. Photochem. Photobiol., A 184 (2006) 93–97.
[32] G.M. Sheldrick, SADABS, University of Göttingen, Germany, 1996.
[33] G.M. Sheldrick, A short history of SHELX, Acta Crystallogr., Sect. A: Found. Crystallogr. 64 (2008) 112–122.
[34] M.A. Spackman, D. Jayatilaka, Hirshfeld surface analysis, CrystEngComm 11 (2009) 19–32.
[35] J.R. Lakowicz, Principles of Fluorescence Spectroscopy, third ed., Plenum, New York, 2006.
[36] U. Pramanik, A.A. Kongasseri, S. Shekhar, A. Mathew, R. Yadav, S. Mukherjee, Structural compactness in hen egg white lysozyme induced by bisphenol S: a spectroscopic and molecular dynamics simulation approach, ChemPhysChem 22 (2021) 1745–1753.
[37] G.M. Morris, D.S. Goodsell, R.S. Halliday, R. Huey, W.E. Hart, R.K. Belew, A.J. Olsen, Automated docking using a Lamarckian genetic algorithm and an empirical binding free energy function, J. Comput. Chem. 19 (1998) 1639–1662.
[38] J. Frisch, G.W. Trucks, H.B. Schlegel, G.E. Scuseria, M.A. Robb, J.R. Cheeseman, G. Scalmani, V. Barone, B. Mennucci, G.A. Petersson, et al., Gaussian 09 Revision E.01, Gaussian Inc., Pittsburg, PA, 2009.
[39] L.L.C. Schrödinger, The PyMOL molecular graphics system, Version~1.8, 2015.
[40] R. Maity, N. Sepay, U. Pramanik, K. Jana, S. Mukherjee, S. Maity, D. Mal, T. Maity, B.C. Samanta, Exploring the noncovalent interactions of the dinuclear Cu (II) Schiff base complex with bovine serum albumin and cell viability against the SiHa cancer cell line, J. Phys. Chem. B 125 (2021) 11364–11373.
[41] N. Margiotta, G. Natile, F. Capitelli, F.P. Fanizzi, A. Boccarelli, P.D. Rinaldis, D. Giordano, M. Coluccia, Sterically hindered complexes of platinum(II) with planar heterocyclic nitrogen donors. A novel complex with 1-methyl-cytosine has a spectrum of activity different from cisplatin and is able of overcoming acquired cisplatin resistance, J. Inorg. Biochem. 100 (2006) 1849–1857.
[42] C. Barbara, P. Orlandi, G. Bocci, A. Fiorovanti, A.D. Paolo, G. Natale, M.D. Tacca, R. Danesi, In vitro and in vivo antitumour effects of novel, orally active bile acid-conjugated platinum complexes on rat hepatoma, Eur. J. Pharmacol. 549 (2006) 27–34.